Desalination and Water Treatment
www.deswater.com

doi: 10.5004/dwt.2022.28279

253 (2022) 285–297
March

Achieving highly efficient growth inhibition on *Microcystis aeruginosa* with location-based lactic acid composites

Mingming Zhan[a,b], Mingjun Ma[a,b], Yu Hong[a,b,*], Chenkang Zhang[a,b], Lihua Li[a,b], Yong Xu[c], Zhilan Zhang[c]

[a]*Beijing Key Lab for Source Control Technology of Water Pollution, College of Environmental Science and Engineering, Beijing Forestry University, Beijing 100083, China, emails: yuhong829908@gmail.com (Y. Hong), 976564222@qq.com (M. Zhan), 2351084057@qq.com (M. Ma), 1052015548@qq.com (C. Zhang), 741763132@qq.com (L. Li)*
[b]*Engineering Research Center for Water Pollution Source Control & Eco-remediation, College of Environmental Science and Engineering, Beijing Forestry University, Beijing 100083, China*
[c]*Shanghai ZEYAO Environmental Technology Co., Ltd., Shanghai 201600, PR China, emails: Xu_yong8899@163.com (Y. Xu), Emily0512@163.com (Z. Zhang)*

Received 22 October 2021; Accepted 8 February 2022

ABSTRACT

Using antialgal allelochemicals to inhibit bloom-forming microalgae is regarded as a promising method to realize effective algal-bloom control. When allelochemicals enter the water body, if their location cannot be effectively controlled, there will be a great negative influence on their inhibitory action, but the related research is rarely reported. In this study, the allelochemical lactic acid (LA) was incorporated into purified diatomite (PD), purified biochar (PB) and magnetic purified expanded perlite (MPEP) to fabricate a heavy composite LA-PD (LA incorporated into PD), a suspended composite LA-PB (LA incorporated into PB) and a floated composite LA-MPEP (LA incorporated into MPEP), and their inhibition effects on the bloom-forming cyanobacterium *Microcystis aeruginosa* were investigated. The results demonstrated that the corresponding growth inhibition rates of 50 mg/L BLA-PD, BLA-PB, and BLA-MPEP (i.e., LA-PD, LA-PB, and LA-MPEP with the best algae inhibition performance) could be up to 100% after 5 d of treatment, and their EC_{50} values were 30.50, 20.87 and 14.02 mg/L, respectively. Co-toxicity coefficient (CTC) was used to evaluate their joint effects of LA and PD, PB, MPEP. The CTC value of BLA-PD was 95.6, indicating an additive effect between LA and PD. The CTC values of BLA-PB and BLA-MPEP were 140.3 and 149.0, which demonstrates synergistic effects between LA and PB, MPEP. The results hint these highly effective composites for location-based algal-bloom control a bright future.

Keywords: Algal blooms; Allelochemicals; Lactic acid; *Microcystis*; Location-directed control

1. Introduction

Algal blooms which frequently break out in eutrophic water bodies and result in deterioration of water quality have raised worldwide concern [1]. Moreover, some microalgae can release algal toxins, posing a serious threat to human health and aquatic life [2]. Therefore, it is urgent and indispensable to explore efficient method for mitigating algal blooms [3]. Physical, chemical and biological methods have been used extensively to eliminate or control the outbreak of algal blooms [4,5]. However, high cost and low efficiency are still bottlenecks hindering the large-scale application of physical methods [6,7]. Chemical methods can effectively and rapidly inhibit algal blooms,

* Corresponding author.

but secondary pollution may largely limit the utilization of chemical methods owing to the toxicity of chemical agents [8,9]. Thus, enormous efforts have been given to biological methods, which are recognized as promising alternatives for suppressing algal blooms [10,11]. Traditional biological approaches still suffered from complex management and poor stability [12,13]. Therefore, it is still urgent to find a suitable biological method with convenient operation and good stability.

Since allelochemicals derived from plants or microorganisms generally have low environmental risks, the allelopathy as one of biological methods has attracted much attention in recent years, and the use of allelochemicals to control algal growth has also become a hot spot [14–16]. Allelochemical substances extracted from many aquatic plants were verified to be very efficient in the inhibition of algal growth, such as lactic acid (LA), tannic acid, pyrogallic acid and gallic acid [17,18]. Wang et al. [19] reported that LA derived from *Potamogeton malaianus* could inhibit the growth of *Microcystis aeruginosa*. Sinang et al. [20] reported that algal cells with the treatment of the allelochemicals extracted from *Melastoma malabathricum*, *Pistia stratiotes*, *Cosmos caudatus* and *Etlingera elatior* showed up to 50%, 42.6%, 35.3%, and 22.5% growth inhibition in contrast with the controls, respectively. Due to the good biodegradability of LA, it has innate potential to control algal blooms in actual water bodies [21]. However, Wen et al. [22] found that the rapid degradation of LA in the water environment also greatly reduced its inhibitory effect on the growth of *Microcystis aeruginosa*. Therefore, how to make the allelochemicals continue to inhibit algae after entering the water body without weakening the effect due to degradation and consumption is also a problem that needs to be considered and solved.

Previous studies have documented that the allelochemical substances embedded within other matrixes could prevent the allelochemicals from consuming aimlessly during application [23–25]. Ni et al. [26] reported that artemisinin encapsulated into alginate-chitosan could exert continuous growth inhibition on *Microcystis aeruginosa* within 30 d. It also has been found that the microalgae treated with 0.2 mg/L lactic acid began to regain rapid growth after 10 d of exposure, while the fatty acid incorporated into chitosan composite microsphere could make *M. aeruginosa* in an inhibited state during the experiment (30 d) [26]. The prolonged antialgal effect is attributed to the protection of LA by the chitosan composite microsphere [27]. Although preventing the rapid loss of allelochemicals through the matrixes is a good way to prolong their effects, controlling the position of allelochemicals in the waterbodies is also very important for the efficient realization of their growth inhibition.

By controlling the density of the packaging matrixes for allelochemicals and following the scenarios before and during the outbreaks of algal blooms, it is possible to realize the positioning of the allelochemicals composite material to control the growth of blooms-forming microalgae in sediment, overlying water, and water surface in the water bodies. Several materials have been used as matrixes employed to encapsulate allelochemicals [28–30]. Especially, expanded perlite (EP), biochar and diatomite have aroused great research interest owing to its large surface area, high porosity, cheap price, and environmental friendliness [31–34]. As is known, EP is obtained by the heat treatment of perlite at 850°C–1,150°C, which is a glassy volcanic holistic rock that could float on the water [35–37]. Biochar is a solid carbon that could suspend in the water body, which was prepared by pyrolyzing plant derived feedstock under limited oxygen supply conditions at 300°C–1,000°C [38]. Diatomite is an earth-abundant siliceous sedimentary rock composed of amorphous silica and could sink to the bottom of the water body [39]. Using EP, biochar, and diatomite to encapsulate allelochemical LA for functional composites fabrication to achieve the fixed-point inhibition of blooms-forming microalgae growth is worthy of research but it has not been reported yet.

In this study, LA was firstly encapsulated into purified diatomite (PD), purified biochar (PB) and magnetic purified expanded perlite (MPEP) to fabricate the sinked (LA-PD), suspended (LA-PB) and floated materials (LA-MPEP), respectively. The surface morphology, surface functional group, thermal stability and composition of the resulting composites were characterized systematically through scanning electron microscopy (SEM), Fourier-transform infrared spectroscopy (FTIR), thermogravimetric analysis (TGA). The algal inhibition performance, the medium effective concentration (EC_{50}) for algal growth inhibition, and the co-toxicity coefficient (CTC) of LA composites were analyzed and evaluated. This research will provide enlightenment and data reference for the development of location-based allelochemicals encapsulated by matrixes.

2. Materials and methods

2.1. Microalgae and culture medium

Microcystis aeruginosa (obtained from Freshwater Algae Culture Collection at the Institute of Hydrobiology, China) was cultivated in the BG 11 medium with a composition of 1,500 mg/L $NaNO_3$, 40 mg/L $K_2HPO_4{\cdot}3H_2O$, 75 mg/L $MgSO_4{\cdot}7H_2O$, 36 mg/L $CaCl_2{\cdot}2H_2O$, 6 mg/L $C_8H_8O_7$, 6 mg/L $C_8H_8O_7$, 6 mg/L $C_6H_8FeNO_7$, 20 mg/L Na_2CO_3, 10 mg/L Na_2EDTA, 2.86 mg/L H_3BO_3, 1.81 mg/L $MnCl_2{\cdot}4H_2O$, 0.22 mg/L $ZnSO_4{\cdot}7H_2O$, 0.079 mg/L $CuSO_4{\cdot}5H_2O$, 0.39 mg/L $Na_2MoO_4{\cdot}2H_2O$, and 0.049 mg/L $Co(NO_3)_2{\cdot}6H_2O$. The microalgae culture solution was autoclaved at 121°C for 30 min. After cooling, algae cells were cultivated in 500 mL Erlenmeyer flask with 300 mL of sterilized culture medium at 24°C–26°C under an irradiance of 40–60 μmol photons m^{-2}/s (12 h light/12 h dark). The flasks were shaken 2–3 times per day, and the algae cells were cultivated to the logarithmic growth phase for further experiments.

2.2. Preparation of the matrix for LA encapsulation

The diatomite was sufficiently ground and placed into porcelain boat, which was heated at 450°C for 6 h under Ar atmosphere. Then 5 g of the powder was added to 50 wt.% H_2SO_4 under magnetic stirring at 500 rpm for 5 h to remove the impurities, then the resulting mixture was filtered, washed with deionized water three times and dried at 60°C for 8 h to obtain the PD.

Biochar was prepared through the high temperature calcination method. Finely ground barley straw powder

was placed in a porcelain boat, which was then put into a muffle furnace and purged with Ar gas by repeated evacuating and filling Ar gas. The boat was heated to 600°C in a current of Ar gas, and maintained at 600°C for 6 h, and the biochar powder was obtained by grinding after cooling to room temperature. Then 5 g of the prepared biochar was then dispersed in 50 wt.% H_2SO_4 with magnetic stirring for 5 h at the speed of 500 rpm. The mixture was filtered, washed with deionized water three times and dried at 60°C for 8 h to obtain the PB.

Typically, 5 g expanded perlite with a diameter 0.5 mm and 50 wt.% H_2SO_4 were mixed in a beaker. The resulting mixture was stirred in the magnetic stirrer for 5 h at the speed of 600 rpm. Then, the PEP was obtained by filtration and further washed with distilled water before they were dried at the temperature of 60°C for 1 h. The prepared PEP (0.5 g) was dissolved in 32 mL ethylene glycol by ultrasonic shaking to obtain a homogeneous suspension. Afterward, 1.08 g of $FeCl_3{\cdot}6H_2O$, 0.80 g polyethylene glycol and 2.88 g CH_3COONa were added into the suspension with magnetic stirring for 10 min at the speed of 400 rpm. The mixture was then transferred to 20 mL Teflon-lined stainless-steel autoclave and went through hydrothermal treatment by heating up to 190°C and lasting for 8 h. After cooling down to room temperature, the black precipitate was collected and washed using ethanol and deionized water three times. Finally, MPEP was obtained by drying at 60°C for 6 h.

2.3. Preparation of LA composites

Co-impregnation method was used for the preparation of LA-PD, LA-PB and LA-MPEP. Typically, 5 g of the PD, 5 g of the PB, and 1 g of the MPEP was separately added in 30 mL lactic acid (Analytical reagent) with magnetic stirring, followed by filtering, washing and drying. The resulting powder was labelled as LA-PD, LA-PB and LA-MPEP, respectively. To identify the optimal preparation condition of the LA nanocomposites, the influencing parameters of the preparation process, including reaction temperature of 50°C, 60°C, 70°C, magnetic stirring speed of 120, 150, 180 rpm and reaction time of 2, 5, 8 h were selected for the $L_9(3^3)$ orthogonal experiment. The detailed information is shown in Fig. S1.

2.4. Characterization of PD, PB, MPEP, and LA composites

The scanning electron microscope (FESEM, SU8010) was applied to investigate the structure of composites. The crystal structure of composites was determined by X-ray diffraction using a D8 ADVANCE, Bruker. The thermal stability of composites was analyzed with TGA using a GA-55 Thermal Gravimetric Analyzer. The surface functional group of the composites was obtained on the Vertex 70 type FTIR Spectrometer.

2.5. Inhibition assay of LA-PD, LA-PB and LA-MPEP on microalgae growth

M. aeruginosa was inoculated into a 300 mL culture medium in a 500 mL Erlenmeyer flask. All flasks were cultivated at under the conditions of 24°C–26°C and 40–60 μmol photons m^{-2}/s (12 h light/12 h dark). Then 4 mg LA-PD, LA-PB and LA-MPEP fabricated from different preparation conditions were added to a 300 mL Erlenmeyer flask containing microalgae with an initial algal density of 5×10^5 cells/mL to obtain the optimal preparation conditions of LA composites with the best algal-inhibition rate, which was labelled as BLA-PD, BLA-PB and BLA-MPEP. Afterward, the concentration gradients of BLA-PD, BLA-PB, and BLA-MPEP were set as 1, 2.5, 5, 10, 25, and 50 mg/L to determine the medium inhibitory concentration (EC_{50}).

Algal cells were counted using hemocytometer under microscope (XSZ-HS3, Chongqing Optoelectronic Instrument Co., Ltd., China) every day. All experiments were repeated three times. Then, the growth inhibition rate (IR) of *M. aeruginosa* was estimated by Eq. (1) [26].

$$\mathrm{IR}(\%) = \frac{N_0 - N_X}{N_0} \times 100 \tag{1}$$

where N_0 is the algal density of the control group, N_X is the algal density of experimental group. The value of IR was employed to calculate EC_{50}. The probit fitting curves were obtained based on the inhibition rate under six concentration conditions at 5 d by probit method [40].

2.6. Joint effect analysis of LA composites in contrast with matrixes and LA

CTC is used to evaluate the joint effect of two exogenous chemicals [41]. In this paper, the joint algal inhibition effects of PD, PB, MPEP, and LA were analyzed by CTC, respectively. The CTC was calculated with the following Eqs. (2)–(5) based on the previous study [42].

$$\mathrm{TI} = \frac{\mathrm{EC}_{50,\mathrm{LA}}}{\mathrm{EC}_{50,\mathrm{Ai}}} \tag{2}$$

$$\mathrm{ATI} = \frac{\mathrm{EC}_{50,\mathrm{LA}}}{\mathrm{EC}_{50,\sum_{i=1}^{i=n}\mathrm{Ai}}} \tag{3}$$

$$\mathrm{TTI} = \sum_{i=0}^{n}\left(\mathrm{TI}_{\mathrm{Ai}} \times \frac{C_{\mathrm{Ai}}}{\sum_{i=0}^{n} C_{\mathrm{Ai}}}\right) \tag{4}$$

$$\mathrm{CTC} = \frac{\mathrm{ATI}}{\mathrm{TTI}} \times 100 \tag{5}$$

where TI represents the toxicity index, ATI represents the actual toxicity index, TTI represents the theoretical toxicity index, Ai represents other material except for LA, C_{Ai} represents the concentration of Ai. If CTC > 120, which is indicative of a synergistic effect; If 80 < CTC < 120, which represents an additive effect; If CTC < 80, which indicates an antagonistic effect [42].

3. Results and discussion

3.1. Growth inhibition effects of LA composites

The influence of the different preparation parameters of LA-PD, LA-PB, LA-MPEP on their growth inhibition effects of *M. aeruginosa* are shown in Fig. 1. As presented in Fig. 1a, the algal density increased with culture time in the control group, which could reach up to 5.95 × 10^6 cells/mL after 7 d. LA-PD had obvious inhibition on *M. aeruginosa* growth. The algal density was only 2.99 × 10^6 cells/mL with the treatment of 13.3 mg/L LA-PD (70°C, 180 rpm, 5 h) at 7 d, the corresponding inhibition rate of *M. aeruginosa* was 49.74% (Fig. 1b), which possessed the best inhibition efficiency compared to the LA-PDs prepared in other conditions. As illustrated in Fig. 1c, LA-PB showed significant suppression against *M. aeruginosa*, and algal cells decreased obviously after exposure to 13.3 mg/L LA-PB. As exposure time extended to 7 d, the algal density could only reach up to 2.97 × 10^6 cells/mL under 13.3 mg/L of LA-PB (50°C, 180 rpm, 8 h), and the corresponding inhibition rate of *M. aeruginosa* was 50.08% (Fig. 1d), which was the highest inhibition ratio among these prepared conditions. The influence of the different preparation parameters of LA-MPEP on its growth inhibition effect were presented in Fig. 1e. The growth inhibitory effects of LA-MPEP could be negligible at 24 h of treatment. The density of the algae began to

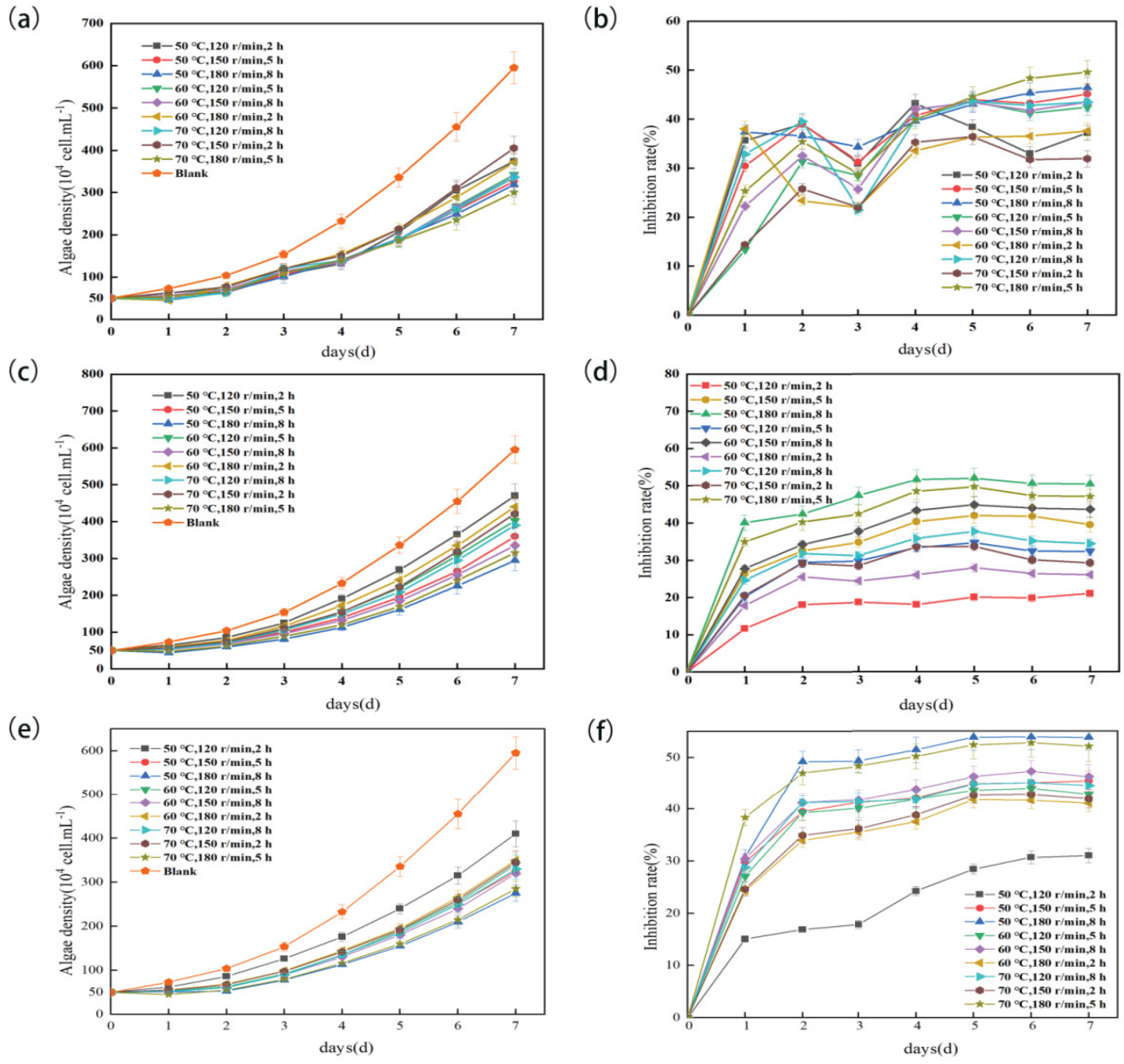

Fig. 1. The influence of the different preparation parameters of BLA-PD (a, b), BLA-PB (c, d), BLA-MPEP (e, f) on their growth inhibition effects.

decline from 48 h, it was 2.75 × 10^6 cells/mL at the dosage of 13.3 mg/L LA-MPEP (50°C, 180 rpm, 8 h) and the inhibition rate was up to 53.78% after 7 d of treatment (Fig. 1f), which was superior to those of LA-MPEPs under other prepared conditions. On the basis of the above results, it could be summarized that the LA-PD (70°C, 180 rpm, 5 h), LA-PB (50°C, 180 rpm, 8 h) and LA-MPEP (50°C, 180 rpm, 8 h) present the best algae inhibition ability, which were labeled as BLA-PD, BLA-PB, and BLA-MPEP, respectively.

3.2. Characterization of LA composites with the best algae inhibition ability

SEM images of PD, PB, MPEP, and LA composites are summarized in Fig. 2. Fig. 2a reveals the abundant pores in the surface of PD, its diameter was approximately 5 nm, and these pores could enable PD to store sufficient LA to suppress the growth of algae. As shown in Fig. 2b, no pores were seen on the surface of BLA-PB, which demonstrated the LA had encapsulated into PD successfully [43]. The SEM image of PB is shown in Fig. 2c, the PB was found to be consisted of the irregular pore, which was an adequate platform for storing LA. As could be seen from Fig. 2d, the hole was hardly observed in BLA-PB, implying that the LA had entered the hole of PB [44]. Fig. 2e presented that MPEP exhibited pentagonal-like pore structure. There was no existence of hole in the SEM image of BLA-MPEP (Fig. 2f), which demonstrated that the formation of LA encapsulation BLA-MPEP [45].

Thermogravimetric (TG) analysis was employed to determine the thermal ability of LA composites. The thermogravimetric (TG) curves of PD, PB, MPEP, LA-PD, LA-PB, and LA-MPEP are shown in Fig. 3. As shown in Fig. 3a, the weight loss for PD from 30°C to 81°C was 3%, which was attributable to the loss of water crystallization. For BLA-PD, the first stage occurred at 30°C–88°C with a weight loss rate

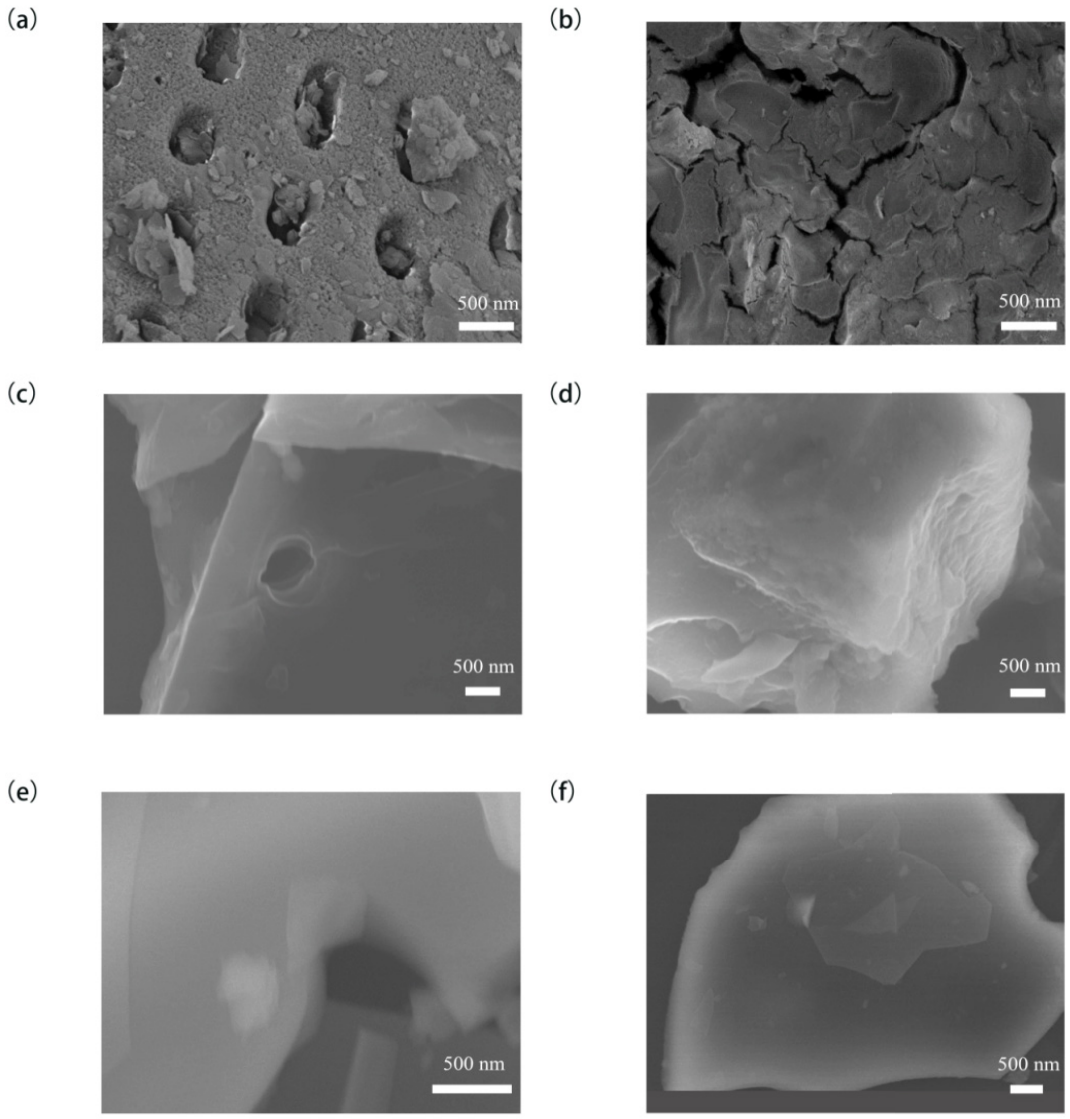

Fig. 2. Scanning electron microscope images of PD (a) and BLA-PD (b), PB (c) and BLA-PB (d), MPEP (e) and BLA-MPEP (f).

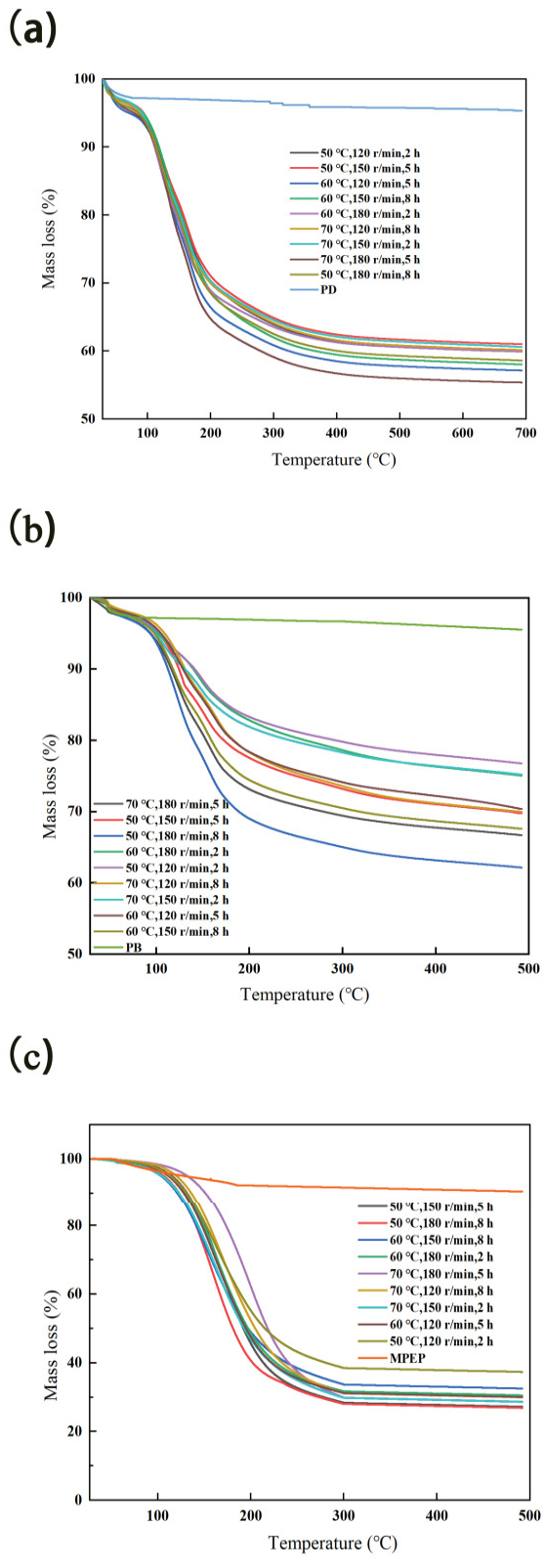

Fig. 3. Thermogravimetric curves of PD, LA-PDs under different preparation parameters (a), PB and LA-PBs under different preparation parameters (b), MPEP and LA-MPEPs under different preparation parameters (c).

of 5.76% is corresponded to the evaporation of free water, crystal water and adsorbed water. The weight loss of the second stage for BLA-PD between 88°C and 342°C (36.44%) was due to the loss of the LA, which contained the largest amount of LA compared with LA-PDs under other preparation parameters. The third stage was observed to occur from 342°C to 493°C mainly because of the burn of carbonaceous residue. In Fig. 3b, the 2.79% weight loss of PB starting at about 31°C and ending at about 78°C was stemmed from the loss of water. The TG curves of BLA-PB could be divided into three stages, the first one (31°C–91°C) with weight loss of 4.43% was associated with the dehydration of the BLA-PB. The second stage (91°C–332°C) accounting for 31.48% of total mass was ascribed to the breakdown of the LA, while the LA content of LA-PBs prepared by other conditions were lower than BLA-PB. The third stage occurred at 332°C–482°C mainly caused by the loss of carbonaceous residue. The TG curves of MPEP and LA-MPEPs under different preparation parameters are shown in Fig. 3c. As illustrated in Fig. 3c, the decrease in mass loss of MPEP was relatively similar to LA-MPEP under different preparation parameters from 52°C to 96°C, which indicated the dehydration of samples [46]. The sharp decline of mass loss occurred from 96°C to 303°C for LA-MPEP under different preparation parameters were corresponded to the decomposition of LA within the LA-MPEP [47]. Compared with LA-MPEPs under other preparation parameters, BLA-MPEP exhibited the largest mass loss at the range of 116°C–218°C (Δm = 68.48%), demonstrating that the best preparation condition was 50°C of reaction temperature, 8 h of time, and 180 rpm of magnetic stirring speed, which was consistent with results from Fig. 3. 1f. In comparison with BLA-PD and BLA-PB, BLA-MPEP possessed the highest LA content, which was likely to have the best inhibition effect on *M. aeruginosa*. The decomposition temperature values of BLA-PD, BLA-PB and BLA-MPEP were much higher than the application temperature, indicating that BLA-PD, BLA-PB and BLA-MPEP had excellent thermal ability at the range of application temperature.

The functional groups of the BLA-PD, BLA-PB and BLA-MPEP were analyzed by FTIR spectra (seen in Fig. 4). As presented in Fig. 4a, for BLA-PD, the adsorption peak located at 1,015 cm^{-1} caused by the stretching vibration of Si–O–Si [48]. The peak at 1,734 cm^{-1} is ascribed to C=O [49]. Additionally, it was also found that the stretching vibration of functional group of C–H at 2,995 and 2,945 cm^{-1} [50]. There was an absorbance peak at 3,331 cm^{-1}, which belonged to the bending vibration of O–H group [51]. Fig. 4b shows the FTIR spectra of BLA-PB, the peak approximately at 1,735 cm^{-1} owing to the stretching vibration of the C=O group [52]. The appearance of the adsorption peaks in the region of 2,900–3,000 cm^{-1} were ascribed to the stretching vibration of the C–H group, which were caused by the CH_2 and CH_3 [53]. The peaks appear at 3,404 cm^{-1} was corresponded to the vibration peak of O–H [54]. For the BLA-MPEP (Fig. 4c), the peak situated at 1,742 cm^{-1} is assigned to C=O [55]. The presence of the peak at 2,939 and 2,990 cm^{-1} reflected the asymmetrical and symmetrical stretching vibration of the C–H group, which were generated by the CH_2 and CH_3 [56]. The band at 3,445 cm^{-1} represented the bending vibration of O–H [57]. The C=O adsorption peak

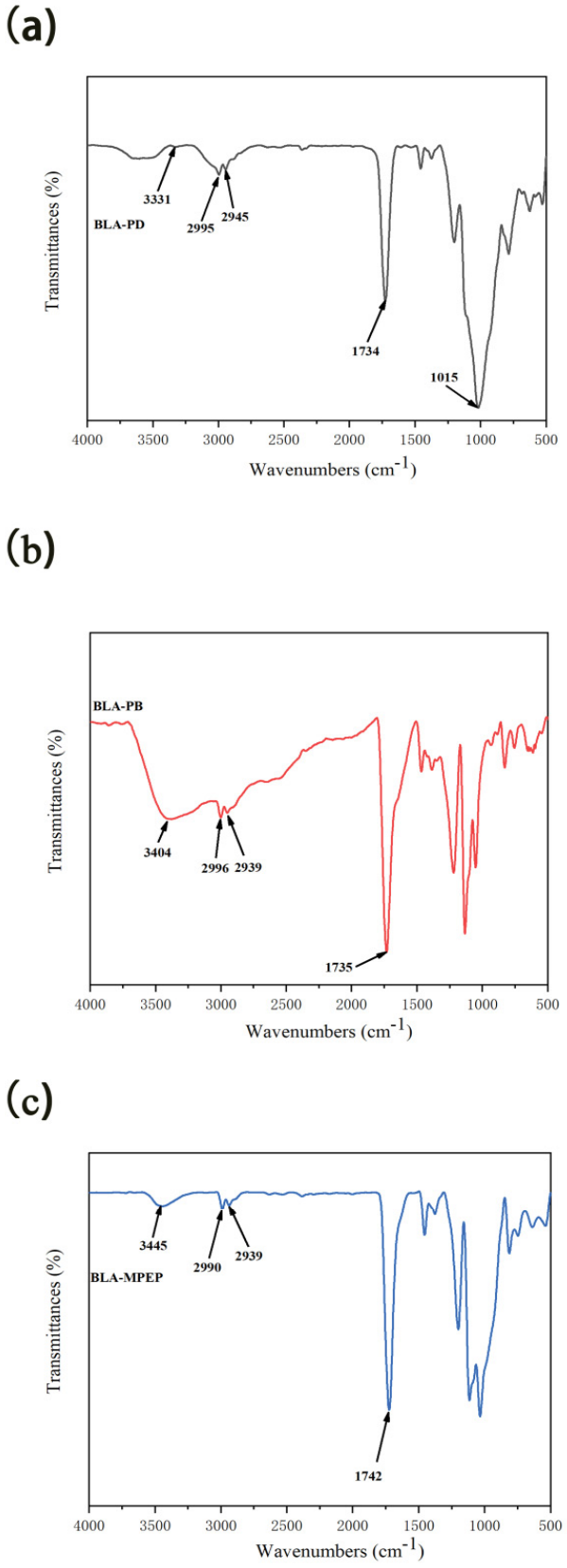

Fig. 4. Fourier-transform infrared spectroscopy of BLA-PD (a), BLA-PB (b), and BLA-MPEP (c).

of lactic acid appeared at 1,730 cm^{-1}, while the C=O characterize peak of BLA-PD, BLA-PB and BLA-MPEP shifts from 1,730 to 1,734, 1,735 and 1,742 cm^{-1}, respectively [58]. In comparison with LA, the red shifts of C=O characterize peak indicated that there were hydrogen bond interactions between the functional groups of PD, PB, MPEP and LA [59]. The interactions such as hydrogen bond and surface tension forces could enable LA easily encapsulated into the holes of the PD, PB, and MPEP, which could prevent the LA leaking from the PD, PB and MPEP to achieve long term inhibition on the growth of algal cells. On the basis of the above results, the BLA-PD, BLA-PB and BLA-MPEP were considered to achieve long term algal inhibition.

3.3. Inhibition effects of LA composites with the best algae inhibition ability on the growth of M. aeruginosa

The histograms of inhibition rate and the probit fitting curves of inhibition rate under different concentrations of BLA-PD, BLA-PB, and BLA-MPEP are shown in Fig. 5. Fig. 5a shows different concentrations of BLA-PD on algae inhibition. In the 1 mg/L BLA-PD treatment group, the inhibition rate of *M. aeruginosa* at 7 d was only 4.98%. When algae cells exposed to 2.5, 5, and 10 mg/L BLA-PD, the inhibition rate were not significantly increasing compared with 1 mg/L BLA-PD. In contrast to the inhibition rate of 1 mg/L BLA-PD, there was an obvious increase when the algae were under 25 and 50 mg/L of BLA-PD. The algae inhibition rate was gradually increasing during 7 d of treatment with 50 mg/L BLA-PD, which was up to 100% after 7 d of treatment. Fig. 5b displays the inhibitory efficiency of 1, 2.5, 5, 10, 25, and 50 mg/L BLA-PB. Algal growth in the treatment with 1 mg/L BLA-PB was slightly suppressed, the algal inhibition rate showed a peak (8.2%) after 3 d of exposure. The inhibition rate increase accompanying with BLA-PB concentration increasing. The highest algae inhibition rate appeared after 7 d of exposure with 50 mg/L of BLA-PB, which was closed to 100% at 7 d. As depicted in Fig. 5c, the algae inhibition rate was improved with an increase in the concentration of BLA-MPEP, and the 50 mg/L BLA-MPEP showed up to nearly 100% inhibition during 4–7 d, which exhibited a more positive inhibition effect when compared with those of 1, 2.5, 5, 10, 25 mg/L BLA-MPEP. The prohibit fitting curves of BLA-PD, BLA-PB, and BLA-MPEP are shown in Figs. 5d–f, respectively. The EC_{50} of BLA-PD was 30.85 mg/L, while those of BLA-PB and BLA-MPEP were 20.87 and 14.02 mg/L, respectively. In a previous report, it was demonstrated that the EC_{50} at 6 d of the allelopathic extracts from *Nelumbo nucifera* stem was 8.79 g/L for *M. aeruginosa* [60]. Deng et al. [61] reported that the EC_{50} of allelochemical dibutyl phthalate extracted from straw on the growth of *M. aeruginosa* at 6 d was 2.1 g/L. Therefore, compared with the *Nelumbo* extracts and dibutyl phthalate, LA composites obviously possessed the lower EC_{50} and higher inhibition efficiency, which had excellent application prospects in the field of usage of allelochemical composites for algae inhibition.

To analyze the algal inhibition effects of BLA-PD, BLA-PB, and BLA-MPEP in contrast with LA, PB, MPEP, and PD, the histograms of inhibition rate and the probit fitting curves of inhibition rate under different concentrations

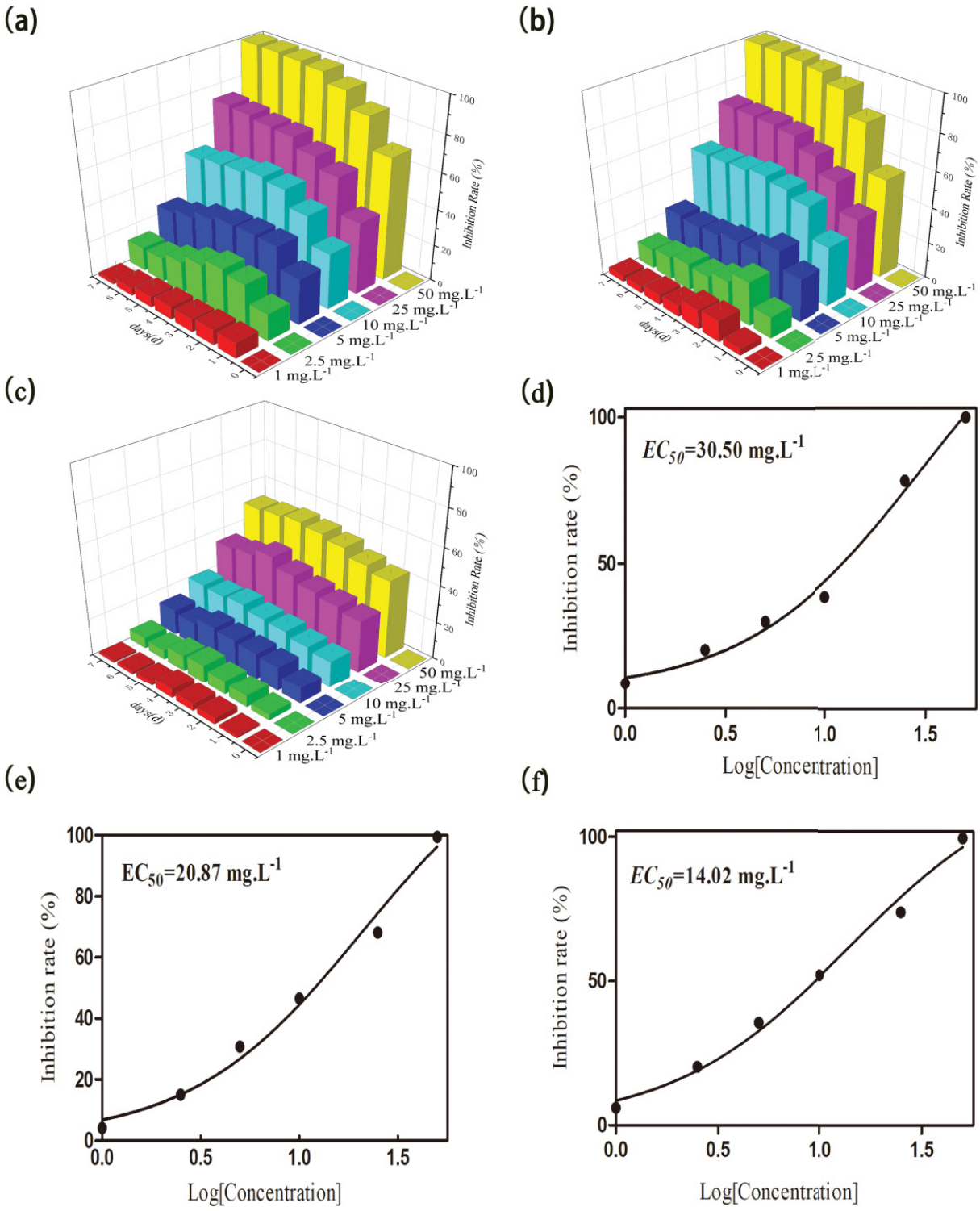

Fig. 5. The histograms of inhibition rate under different concentrations of BLA-PD (a), BLA-PB (b), BLA-MPEP (c) on algae inhibition; The probit fitting curve of inhibition rate under different concentrations of BLA-PD (d), BLA-PB (e), BLA-MPEP (f).

of PD, PB, and MPEP were also investigated (shown in Supporting Information). As shown in Fig. S1, the 50 mg/L LA had the best algal inhibition ability, the inhibition rate was close to 100% at 7 d, and the corresponded EC_{50} of LA was 19.83 mg/L. Fig. S2 shows the influence of different concentrations of PD on algae inhibition and probit fitting curve of PD, the PD has relatively low anti-algae effect, the optimal inhibition rate achieved by 50 mg/L PD at 5 d was

51.59%, which was much lower than that of the LA and BLA-PD, and the EC_{50} of PD was 39.87 mg/L. It was observed that 50 mg/L PB at 5 d was 50.89%, and the EC_{50} of PB was 37.48 mg/L (Fig. S3). As shown in Fig. S4, the highest inhibition rate of MPEP was 52.83% and the EC_{50} of MPEP was 23.65 mg/L. Based on the results, the PD, PB and MPEP had weak inhibition effect on algae cells, which indicated that the LA within BLA-PD, BLA-PB, and BLA-MPEP played a vital role in the process of algae inhibition. Additionally, BLA-MPEP possessed superior algae inhibition ability compared to the other two, which may be attributed to its largest LA content per package.

CTC is used to evaluate the joint algal inhibition effects of PD, PB, MPEP, and LA. Table 1 shows the CTC value of BLA-PD, BLA-PB and BLA-MPEP (detailed CTC calculation process in Supporting Information 5). Xu et al. [62] founded a synergistic effect of bt and an chlorbenzuron mixture on *Hyphantria cunea* Drury, which could effectively improve the toxicity of chlorbenzuron on the *H. cunea*. Chen et al. [42] reported that the methoxyfenozide and lufenuron exhibited optimum synergistic toxicity on *Spodoptera exiguaata* mass ratio of 4:6, and the CTC value was 165.705. The CTC values of BLA-PD, BLA-PB, BLA-MPEP were 95.6, 140.3, 149.0, respectively. The result demonstrated that an additive or synergistic effect between LA and PD, PB, MPEP, which was beneficial to suppress the growth of algae.

4. Conclusions

In this study, the heavy composite BLA-PD, the suspended composite BLA-PB, and the floated composite BLA-MPEP were prepared by incorporating lactic acid (LA) into purified diatomite (PD), purified biochar (PB), and magnetic purified expanded perlite (MPEP) using co-impregnation method. SEM images pointed out that LA had introduced into PD, PB and MPEP. Thermogravimetric analysis results displayed that the BLA-PD, BLA-PB, and BLA-MPEP possessed outstanding thermal ability at the range of application temperature. FTIR spectra further confirmed that the LA had introduced into PD, PB and MPEP. The algae inhibition assay showed that inhibition actions of BLA-PD, BLA-PB, and BLA-MPEP were superior to those of LA, PD, PB, and MPEP. The CTC values of BLA-PD (95.6), BLA-PB (140.3), and BLA-MPEP (149.0) indicated additive or synergistic effects between LA and PD, LA and PB, LA and MPEP. To develop lactic acid-encapsulating composites BLA-PD, BLA-PB, and BLA-MPEP for bottom-mud, overlying water, and water surface directed algal-bloom prevention and control will have a great application potential.

Acknowledgments

This research was supported by the National Natural Science Foundation of China (No.52071030), the Scientific Research Project supported by Enterprise (No. 2020-HXFW-HJ-0004), and the Fundamental Research Funds for the Central Universities (No. 2021ZY75). The authors acknowledge Prof. Hongying Hu (Tsinghua University) and Prof. Yanglong Hou (Peking University) for the technical assistance.

References

[1] X. Li, S. Peng, X. Deng, M. Su, H. Zeng, Attribution of lake warming in four shallow lakes in the middle and lower Yangtze river basin, Environ. Sci. Technol., 53 (2019) 12548–12555.
[2] X. Hu, X.J. Hu, C.F. Tang, S.Z. Wen, X.F. Wu, J. Long, X. Yang, H. Wang, L. Zhou, Mechanisms underlying degradation pathways of Microcystin-LR with doped TiO_2 photocatalysis, Chem. Eng. J., 330 (2017) 355–371.
[3] P.R. Liu, T. Wang, Z.Y. Yang, Y. Hong, X. Xie, Y.L. Hou, Effects of Fe_3O_4 nanoparticle fabrication and surface modification on *Chlorella* sp. harvesting efficiency, Sci. Total Environ., 704 (2019) 135286, doi: 10.1016/j.scitotenv.2019.135286.
[4] D. Liu, P. Wang, G.R. Wei, W.B. Dong, F. Hui, Removal of algal blooms from freshwater by the coagulation–magnetic separation method, Environ. Sci. Pollut. Res., 20 (2013) 60–65.
[5] J.K. Song, X.J. Wang, J.X. Ma, X. Wang, J.Y. Wang, J.F. Zhao, Visible-light-driven in situ inactivation of *Microcystis aeruginosa* with the use of floating g-C_3N_4 heterojunction photocatalyst: performance, mechanisms and implications, Appl. Catal., B, 226 (2017) 83–92.
[6] H.R. Sindelar, J.N. Yap, T.H. Boyer, M.T. Brown, Algae scrubbers for phosphorus removal in impaired waters, Ecol. Eng., 85 (2015) 144–158.
[7] Y. Tang, H. Zhang, X. Liu, D.Q. Cai, H.Y. Feng, C.G. Miao, X.Q. Wang, Z.Y. Wu, Z.L. Yu, Flocculation of harmful algal blooms by modified attapulgite and its safety evaluation, Water Res., 45 (2011) 2855–2862.
[8] K.P. Tsai, H. Uzun, H. Chen, T. Karanfil, A.T. Chow, Control wildfire-induced *Microcystis aeruginosa* blooms by copper sulfate: trade-offs between reducing algal organic matter and promoting disinfection by-product formation, Water Res., 158 (2019) 227–236.
[9] Y.J. Sun, H.L. Zheng, Z.P. Xiong, Y.L. Wang, X.M. Tang, W. Chen, Y. Ding. Algae removal from raw water by flocculation and the fractal characteristics of flocs, Desal. Water Treat., 56 (2015) 894–904.
[10] B.H. Zhang, Z.G. Ding, H.Q. Li, X.Z. Mou, Y.Q. Zhang, J.Y. Yang, E.M. Zhou, W.J. Li, Algicidal activity of *Streptomyces eurocidicus* JXJ-0089 metabolites and their effects on microcystis physiology, Appl. Environ. Microbiol., 82 (2016) 5132–5143.
[11] H. Zou, J.X. Deng, Y. Zhu, Application of plant allelopathy in controlling of algal bloom, Food Sci. Biotechnol., 31 (2012) 134–140.
[12] Y.L. Guo, H.Y. Fu, G.H. Huang, P.F. Gao, T. Chai, B. Yan, H. Liao, Allelopathy effects of ferulic acid and coumarin on *Microcystis aeruginosa*, Environ. Sci., 34 (2013) 1492–1497.
[13] B.L. Wang, Q.Y. Song, J.J. Long, J.F. Song, W.J. Mi, Y.H. Bi, Optimization method for *Microcystis* bloom mitigation by hydrogen peroxide and its stimulative effects on growth of chlorophytes, Chemosphere, 228 (2019) 503–512.
[14] H.P. Wang, F. Liu, P. Luo, Z.H. Li, L.G. Zheng, H. Wang, D.S. Zou, J.S. Wu, Allelopathic effects of *Myriophyllum aquaticum* on two cyanobacteria of *Anabaena flos-aquae* and *Microcystis aeruginosa*, Bull. Environ. Contam. Toxicol., 98 (2017) 556–561.
[15] S.P. Zuo, Z.C. Fang, S.B. Zhou, L.T. Ye, Benthic fauna promote algicidal effect of allelopathic macrophytes on *Microcystis aeruginosa*, J. Plant Growth Regul., 35 (2016) 646–654.
[16] S.P. Zuo, H.M. Wang, L.D. Gan, L.D.D. Gan, M.H. Shao, Allelopathy appraisal of worm metabolites in the synergistic effect between *Limnodrilus hoffmeisteri* and *Potamogeton malaianus* on algal suppression, Ecotoxicol. Environ. Saf., 182 (2019) 109482.
[17] P. Laue, H. Bährs, S. Chakrabarti, C.E.W. Steinberg, Natural xenobiotics to prevent cyanobacterial and algal growth in freshwater: contrasting efficacy of tannic acid, gallic acid, and gramine, Chemosphere, 104 (2014) 212–220.
[18] Z.B. Wu, Y.N. Gao, J. Wang, B.Y. Liu, Y.Y. Zhang, Allelopathic effects of pyrogallic acid secreted by submerged macrophytes on *Microcystis aeruginosa*: role of ROS generation, Allelopathy J., 33 (2014) 121–129.
[19] H.Q. Wang, S.P. Cheng, S.H. Zhang, H. Feng, L. Wei, L.P. Zhang, C.Y. Hu, F.J. Ge, Z.B. Wu, Chemical composition in aqueous

extracts of *Potamogeton malaianus* and *Potamogeton maackianus* and their allelopathic effects on *Microcystis aeruginosa*, Pol. J. Environ. Stud., 19 (2010) 213–218.
[20] S.C. Sinang, N. Daud, N. Kamaruddin, K.B. Poh, Potential growth inhibition of freshwater algae by herbaceous plant exctracts, Acta Ecol. Sin., 39 (2019) 229–233.
[21] O.R. Colegio, N.Q. Chu, A.L. Szabo, T. Chu, A.M. Rhebergen, V. Jairam, N. Cyrus, C.E. Brokowski, S.C. Eisenbarth, G.M. Phillips, Functional polarization of tumour-associated macrophages by tumour-derived lactic acid, Nature, 513 (2014) 559–563.
[22] Z. Wen, H. Yan, M. Shi, B. Chen, T.T. Zhang, Inhibitory effect of the lactic acid leaching solution of *Allium cepa* L. on *Microcystis aeruginosa*, J. Hyg., 47 (2018) 822–832.
[23] H.J. Tian, J.J. Du, J. Wen, Y. Liu, S.R. Montgomery, T.P. Scott, B. Aghdasiet, C.J. Xiong, A. Suzuki, T. Hayashi, M. Ruangchainikom, K. Phan, G. Weintraud, A. Raed, S.S. Murray, M.D. Doubs, X.J. Yang, X.B. Yuan, J.C. Wang, Y.F. Lu, Growth-factor nanocapsules with tunable release capability for bone regeneration, ACS Nano, 10 (2016) 7362–7369.
[24] S.E. Bae, J. Choi, Y.K. Joung, K. Park, D.K. Han, Controlled release of bone morphogenetic protein (BMP)-2 from nanocomplex incorporated on hydroxyapatite-formed titanium surface, J. Control Release, 160 (2012) 676–684.
[25] A. Sar, A. Karaipekli, C. Alkan, Preparation, characterization and thermal properties of lauric acid/expanded perlite as novel form-stable composite phase change material, Chem. Eng. J., 155 (2009) 899–904.
[26] L.X. Ni, K. Acharya, G.X. Ren, S.Y. Li, Y.P. Li, Y. Li, Preparation and characterization of anti-algal sustained-release granules and their inhibitory effects on algae, Chemosphere, 91 (2013) 608–615.
[27] L.X. Ni, X.T. Jie, P.F. Wang, S.Y. Li, S.Z. Hu, Y.P. Li, Y. Li, K. Acharya, Characterization of unsaturated fatty acid sustained-release microspheres for long-term algal inhibition, Chemosphere, 120 (2015) 383–390.
[28] A. Sar, A. Karaipekli, K. Kaygusuz, Capric acid and stearic acid mixture impregnated with gypsum wallboard for low-temperature latent heat thermal energy storage, Int. J. Energy Res., 32 (2008) 154–160.
[29] A. Belščak-Cvitanović, R. Stojanović, V. Manojlović, D. Komes, I.J. Cindrić, V. Nedović, B. Bugarski, Encapsulation of polyphenolic antioxidants from medicinal plant extracts in alginate–chitosan system enhanced with ascorbic acid by electrostatic extrusion, Food Res. Int., 44 (2011) 1094–1101.
[30] A. Karaipekli, A. Sari, Capric-myristic acid/vermiculite composite as form-stable phase change material for thermal energy storage, Sol. Energy, 83 (2009) 323–332.
[31] F. Cheng, X.G. Zhang, R.L. Wen, Z.H. Huang, M.H. Fang, Y.G. Liu, X.W. Wu, X. Min, Thermal conductivity enhancement of form-stable tetradecanol/expanded perlite composite phase change materials by adding Cu powder and carbon fiber for thermal energy storage, Appl. Therm. Eng., 156 (2019) 653–659.
[32] U.A. Khan, J.J. Liu, J.B. Pan, H.C. Ma, S.L. Zuo, Y.C. Yu, A. Ahmad, S. Ullah, M. Iqbal, B.S. Li, Fabrication of flower-shaped hierarchical rGO QDs-Bi-Bi_2WO_6/EP floating photocatalyst: eminent degradation kinetic under sun-like irradiation, Appl. Surf. Sci., 484 (2019) 341–353.
[33] J. Meng, L.L. Wang, X.M. Liu, J.J. Wu, P.C. Brookes, J.M. Xu, Physicochemical properties of biochar produced from aerobically composted swine manure and its potential use as an environmental amendment, Bioresour. Technol., 142 (2013) 641–646.
[34] Z. Wang, Y. Lin, D.Y. Wu, H.N. Kong, Hydrous iron oxide modified diatomite as an active filtration medium for phosphate capture, Chemosphere, 144 (2016) 1290–1298.
[35] C.Z. Liu, C.Y. Luo, T.T. Xu, P.Z. Lv, Z.H. Rao, Experimental study on the thermal performance of capric acid-myristyl alcohol/expanded perlite composite phase change materials for thermal energy storage, Sol. Energy, 191 (2019) 585–595.
[36] W.J. Long, X.W. Tan, B.X. Xiao, N.X. Han, F. Xing, Effective use of ground waste expanded perlite as green supplementary cementitious material in eco-friendly alkali activated slag composites, J. Cleaner Prod., 213 (2019) 406–414.
[37] L.L. Fu, Q.H. Wang, R.D. Ye, X.M. Fang, Z.G. Zhang, A calcium chloride hexahydrate/expanded perlite composite with good heat storage and insulation properties for building energy conservation, Renewable Energy, 114 (2017) 733–743.
[38] C.C. Qin, H. Wang, X.Z. Yuan, T. Xiong, J.J. Zhang, J. Zhang, Understanding structure–performance correlation of biochar materials in environmental remediation and electrochemical devices, Chem. Eng. J., 382 (2019) 122977, doi: 10.1016/j.cej.2019.122977.
[39] R.J. Zheng, Z.J. Ren, H.M. Gao, A.L. Zhang, Z. Bian, Effects of calcination on silica phase transition in diatomite, J. Alloys Compd., 757 (2018) 364–371.
[40] R. Maryam, A. Nusret, An investigation on the toxic effects of Malathion (Organophosphate Insecticide) on the *Daphnia magna Straus*, 1820 (Crustacea, Cladocera), Turk. J. Zool., 26 (2002) 349–349.
[41] J. Li, L. Jiang, Y.W. Zhang, G. Qiang, S.C. Han, Study of a new biological control method combining an enteropathogen and a chemical insecticide against *Solenopsis invicta* (Hymenoptera: Formicidae), J. Econ. Entomol., 111 (2018) 817–822.
[42] J.X. Chen, W.L. Jiang, H.Y. Hu, X.Y. Ma, Q. Li, X.P. Song, X.L. Ren, Y. Ma, Joint toxicity of methoxyfenozide and lufenuron on larvae of *Spodoptera exigua* Hübner (Lepidoptera: Noctuidae), J. Asia-Pac. Entomol., 22 (2018) 795–801.
[43] X.G. Zhang, Z.Y. Yin, D.Z. Meng, Z.H. Huang, R.L. Wen, Y.T. Huang, X. Min, Y.G. Liu, M.H. Fang, X.W. Wu, Shape-stabilized composite phase change materials with high thermal conductivity based on stearic acid and modified expanded vermiculite, Renewable Energy, 112 (2017) 113–123.
[44] Y.F. Xu, X.G. Zhang, B.G. Wu, Y.G. Xu, R.L. Wen, Y.G. Liu, M.H. Fang, X.W. Wu, X. Min, Z.H. Huang, Preparation and performance of shape-stable phase change materials based on carbonized-abandoned orange peel and paraffin, Fullerenes Nanotubes Carbon Nanostruct., 27 (2018) 289–298.
[45] X.G. Zhang, R.L. Wen, C. Tang, B.G. Wu, Z.H. Huang, X. Min, Y.T. Huang, Y.G. Liu, M.H. Fang, X.W. Wu, Thermal conductivity enhancement of polyethylene glycol/expanded perlite with carbon layer for heat storage application, Energy Build., 130 (2016) 113–121.
[46] E.A. Faria, A.G.S. Prado, Kinetic studies of the thermal degradation of cellulose acetate/niobium and chitosan/niobium composites, React. Funct. Polym., 67 (2007) 655–661.
[47] F. Chen, M. Tian, D.M. Zhang, J. Wang, Q.G. Wang, X.X. Yu, X.H. Zhang, C.X. Wan, Preparation and characterization of oxidized alginate covalently cross-linked galactosylated chitosan scaffold for liver tissue engineering, Mater. Sci. Eng., 32 (2012) 310–320.
[48] S. Karaman, A. Karaipekli, A. Sar, A. Bicer, Polyethylene glycol (PEG)/diatomite composite as a novel form-stable phase change material for thermal energy storage, Sol. Energy Mater. Sol. Cells, 95 (2011) 1647–1653.
[49] N. Tudorachi, R. Lipsa, F.R. Mustata, Thermal degradation of carboxymethyl starch-g-poly(lactic acid) copolymer by TG–FTIR–MS analysis, Ind. Eng. Chem. Res., 51 (2012) 15537–15545.
[50] N. Karimpour-Motlagh, H.A. Khonakdar, S.M.A. Jafari, M. Panahi-Sarmad, S.F. Kasbi, S. Shojaei, V. Goodarzih, M. Arjmand, Influence of polypropylene and nanoclay on thermal and thermo-oxidative degradation of poly(lactide acid): TG-FTIR, TG-DSC studies and kinetic analysis, Thermochim. Acta, 691 (2020) 178709, doi: 10.1016/j.tca.2020.178709.
[51] C.G.D. Rosa, C.D. Borges, R.C. Zambiazi, M.R. Nunes, E.V. Benvenutt, S.R.D. Luz, R.F. Davila, J.K. Rutz, Microencapsulation of gallic acid in chitosan, β-cyclodextrin and xanthan, Ind. Crops Prod., 46 (2013) 138–146.
[52] S.H. Yu, F.L. Mi, J.C. Pang, S.C. Jiang, T.H. Kuo, S.J. Wu, S.S. Shyu, Preparation and characterization of radical and pH-responsive chitosan–gallic acid conjugate drug carriers, Carbohydr. Polym., 84 (2011) 794–802.
[53] L.Y. Ma, C.G. Guo, R.X. Ou, L.C. Sun, Q.W. Wang, L.P. Li, Preparation and characterization of modified porous wood flour/lauric-myristic acid eutectic mixture as a form-stable phase change material, Energy Fuels, 32 (2018) 5453–5461.
[54] S.S. Khemalapure, V.S. Katti, C.S. Hiremath, M. Basanagouda, S.M. Hiremath, S.J. Armakovic, S. Armakovic, Molecular

structure, optoelectronic properties, spectroscopic (FTIR, FT-Raman and UVeVis), H-BDE, NBO and drug likeness investigations on 7,8-benzocoumarin-4-acetic acid (7BAA), J. Mol. Struct., 1195 (2019) 815–826.
[55] C.Y. Guo, X.F. Luo, X.H. Zhou, B.J. Shi, J.J. Wang, J. Zhao, J.J. Wang, Quantitative analysis of binary polymorphs mixtures of fusidic acid by diffuse reflectance FTIR spectroscopy, diffuse reflectance FT-NIR spectroscopy, Raman spectroscopy and multivariate calibration, J. Pharm. Biomed., 140 (2017) 130–136.
[56] A. Shalviri, Q. Liu, M.J. Abdekhodaie, X.Y. Wu. Novel modified starch–xanthan gum hydrogels for controlled drug delivery: synthesis and characterization, Carbohydr. Polym., 79 (2010) 898–907.
[57] S.M. Hiremath, A. Suvitha, N.R. Patil, C.S. Hiremath, S.S.K. Khemalapure, S.K. Pattanayak, Molecular structure, vibrational spectra, NMR, UV, NBO, NLO,HOMO-LUMO and molecular docking of 2-(4,6-dimethyl-1-benzofuran-3-yl) acetic acid (2DBAA): experimental and theoretical approach, J. Mol. Struct., 1171 (2018) 362–374.
[58] X.Y. Dou, Q. Li, Q.X. Wu, L.S. Duan, S.Y. Zhou, Y. Zhang, Effects of lactic acid and mixed acid aqueous solutions on the preparation, structure and properties of thermoplastic chitosan, Eur. Polym. J., 134 (2020) 109850, doi: 10.1016/j.eurpolymj.2020.109850.
[59] J.S. Liu, Y.Y. Yu, X. He, Research on the preparation and properties of lauric acid/expanded perlite phase change materials, Energy Build., 110 (2016) 108–111.
[60] L.S. He, F.L. Meng, X.J. Diao, Y.W. Li, R. Meng, B.D. Xi, J.M. Shu, Allelopathic effect of *elumbo nucifera* stem and leaf tissue extract on the growth of *Microcystis aeruginosa* and *Scenedesmus quadricanda*, Environ. Sci., 34 (2013) 2637–2641.
[61] J.X. Deng, H. Zou, Y. Zhuang, On the isolation of anti-algal compounds from the wheat straw and the algae inhibiting effect, J. Saf. Environ., 13 (2013) 39–43.
[62] M. Xu, F.Y. Xu, X.Q. Wu, Effects of the activity of midgut chitinase, cuticle ache on 4th instar larvae of *Hyphantria cunea* by the treatment of different concentration of the mixture of bt and chlorbenzuron, J. Southwest For. Univ., 35 (2015) 64–70.

Supplementry Information

Table S1
Orthogonal experimental factors design for LA-PD, LA-PB and LA-MPEP

Factors	Temperature (°C)	Speed (r/min)	Time (h)
1	50	120	2
2	50	150	5
3	50	180	8
4	60	120	5
5	60	150	8
6	60	180	2
7	70	120	8
8	70	150	2
9	70	180	5

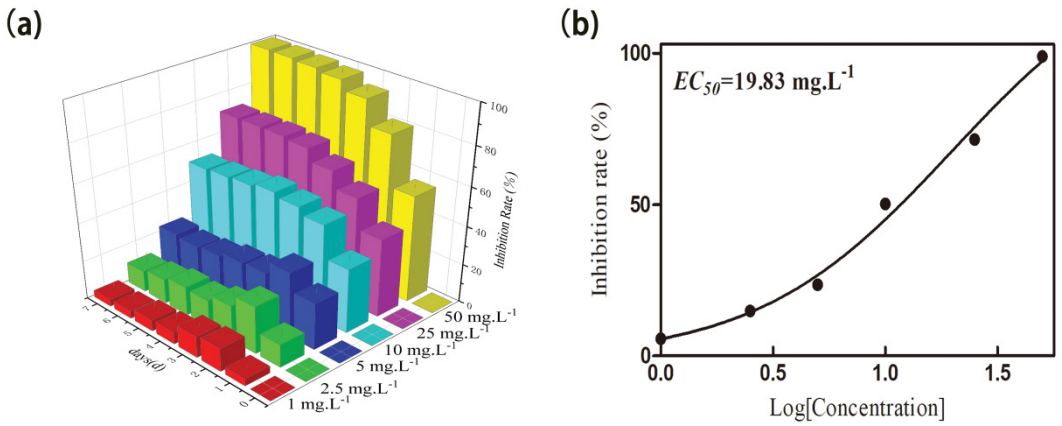

Fig. S1. Influence of different concentrations of LA on algae inhibition (a) and probit fitting curve of LA (b).

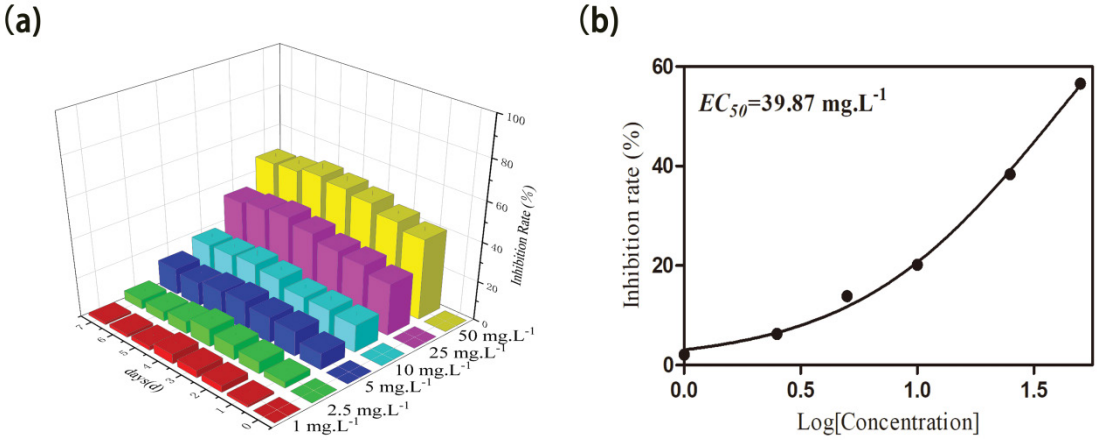

Fig. S2. Influence of different concentrations of PD on algae inhibition (a) and probit fitting curve of PD (b).

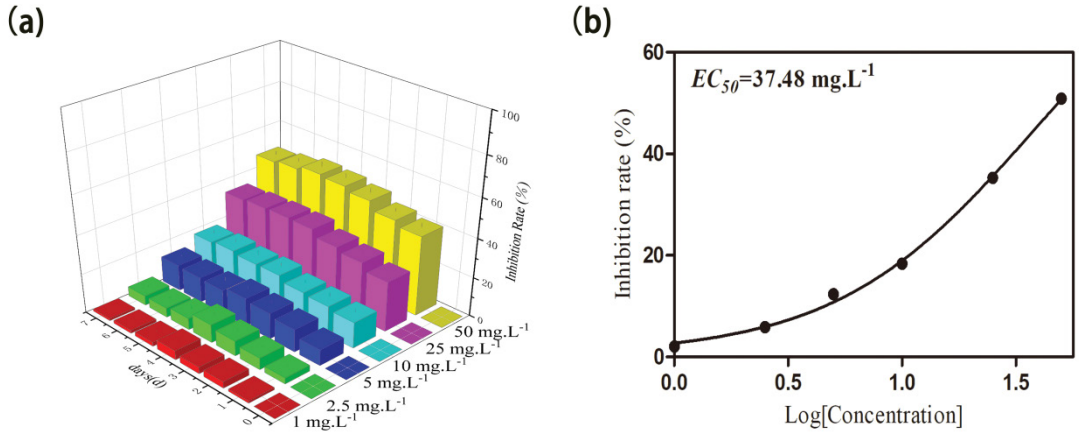

Fig. S3. Influence of different concentrations of PB on algae inhibition (a) and probit fitting curve of PB (b).

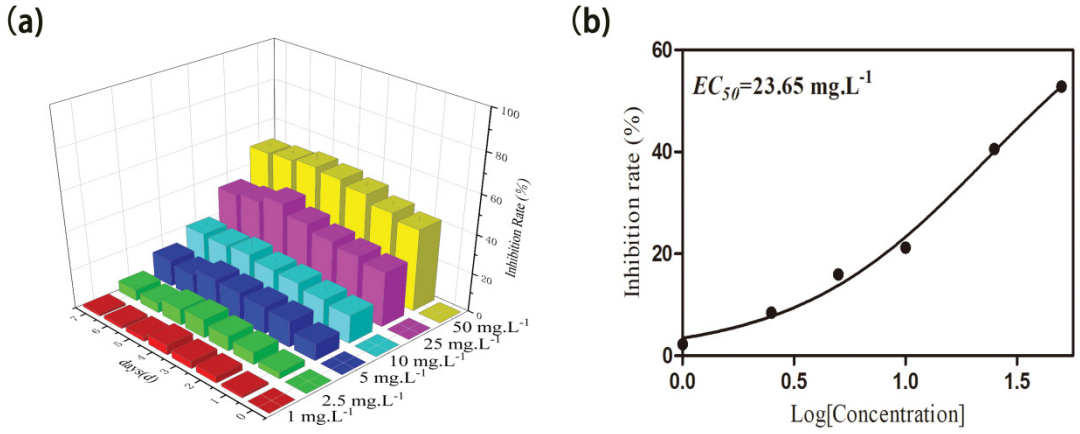

Fig. S4. Influence of different concentrations of MPEP on algae inhibition (a) and probit fitting curve of MPEP (b).

In this paper, LA was selected as a standard material, the CTC value of theBLA-PD, BLA-PB and BLA-MPEP were calculated as follows:

BLA-PD:

$TI_{LA} = EC_{50\ LA}/EC_{50\ LA} \times 100 = 100$

$TI_{LA} = EC_{50\ LA}/EC_{50\ LA} \times 100 = 19.83/39.87 \times 100 = 49.7$

ATI = 19.83/30.50 × 100 = 65.0

TTI = 100 × 0.364 + 49.7 × 0.636 = 68.0

CTC = ATI/TTI × 100 = 65.0/68.0 × 100 = 95.6

BLA – PB:

$TI_{LA} = EC_{50\ LA}/EC_{50\ LA} \times 100$=100

$TI_{PD} = EC_{50\ LA}/EC_{50\ PB} \times 100 = 19.83/37.48 \times 100$=52.9

ATI = 19.83/20.87 × 100 = 95.0

TTI = 100 × 0.315 + 52.9 × 0.685 = 67.7

CTC = ATI/TTI × 100 = 95.0/67.7 × 100 = 140.3

BLA – MPEP:

$TI_{LA} = EC_{50\ LA}/EC_{50\ LA} \times 100 = 100$

$TI_{MPEP} = EC_{50\ LA}/EC_{50\ MPEP} \times 100 = 19.83/23.65 \times 100 = 83.8$

ATI = 19.83/14.02 × 100 = 141.4

TTI = 100 × 0.685 + 83.80 × 0.315 = 94.9

CTC = ATI/TTI × 100 = 141.4/94.9 × 100 = 149.0